Catalysis Science & Technology

Low quantum efficiency of μ-oxo iron bisporphyrin photocatalysts explained with femtosecond M-edge XANES

Journal:	*Catalysis Science & Technology*
Manuscript ID	CY-ART-06-2022-001081.R1
Article Type:	Paper
Date Submitted by the Author:	21-Aug-2022
Complete List of Authors:	Sye, Kori; University of Illinois at Urbana-Champaign, Department of Chemistry Leahy, Clare; University of Illinois at Urbana-Champaign, Chemistry Vura-Weis, Josh; University of Illinois at Urbana-Champaign, Department of Chemistry

ARTICLE

Low quantum efficiency of μ-oxo iron bisporphyrin photocatalysts explained with femtosecond M-edge XANES

Received 00th January 20xx,
Accepted 00th January 20xx

DOI: 10.1039/x0xx00000x

Kori M. Sye,[a†] Clare A. Leahy, [a†] and Josh Vura-Weis [a]

Bridged μ-oxo iron porphyrins serve as photocatalysts for oxidative organic transformations, but suffer from low photon-to-product efficiency. This low photochemical quantum yield is most commonly attributed to the short lifetime of a disproportionated TPPFe(II)/TPPFe(IV)=O state, but an alternate hypothesis suggests that the majority photoproduct is a catalytically inactive ligand-centered TPPFe(III)$^+$/TPPFe(III)-O$^-$ ion pair. We use femtosecond optical and extreme ultraviolet (XUV) spectroscopy to investigate the early photodynamics of the μ-oxo iron bisporphyrin $(TPPFe)_2O$ and identify the primary loss mechanism. XUV spectroscopy probes 3p→3d transitions, corresponding to $M_{2,3}$-edge XANES spectra, and is a distinctive probe of the metal oxidation state. Excitation of the mixed π-π*/ligand-to-metal charge transfer (LMCT) band results in the formation of an iron(II)/iron(III) LMCT state in tens of femtoseconds. This state decays on a subpicosecond timescale to the ligand-centred iron(III) ion pair state, and no TPPFe(IV)=O species is observed within the sensitivity of the measurement. The lack of an iron(II)/iron(IV) XANES spectrum suggests that preferential formation of the inactive iron(III) ion pair state is a main cause of the low quantum yield of this and similar bisporphyrins.

Introduction

Porphyrins and metalloporphyrins serve as an excellent synthetic mimic of biological photo-harvesters and active sites in metalloenzymes, and thus have been of great interest in the development of photocatalysts in important organic transformations. Iron(III) porphyrins have been widely studied as promising earth-abundant, atom-efficient oxidation catalysts.[1,2] In particular, bridging μ-oxo iron bisporphyrins serve as photocatalysts for oxygen atom transfer (OAT), taking advantage of the porphyrin ligand photoactivity and bimetallic cooperativity to generate a reactive iron(IV)-oxo centre using molecular dioxygen (O_2) as the terminal oxidant. These systems are effective for photooxidation of substrates such as hydrocarbons and alkenes.[1–6] However, the quantum yields (Φ, product formed vs photons absorbed) for these systems are generally poor (≤10^{-4}) and thus limit their practical use.[4] For example, every photoexcitation that does not lead to the desired product will heat the reaction vessel, bleach the photocatalyst, and/or catalyse an unwanted side product.

This low quantum efficiency has led to speculation about the excited state dynamics of these complexes. Based on picosecond optical transient absorption (OTA) of a simple bisporphyrin, μ-oxo bis[tetraphenylporphyrinato iron(III)] ($(TPPFe)_2O$, Figure 1A), two main competing pathways have been proposed for the photochemistry of these systems after ligand-to-metal charge transfer (LMCT) excitation. In the first proposal (pathway A in Figure 1B), one of the Fe-O bonds of the μ-oxo bridge undergoes a homolytic cleavage and separates into the reactive iron(IV)-oxo, TPPFe(IV)=O, and a bare TPPFe(II).[4] The Fe(IV)-oxo subsequently reacts with the desired substrate to give the oxidized product. The original catalyst can then be reformed after the TPPFe(II) subunits react with O_2, allowing for efficient substrate oxidation using a readily accessible O-atom source and light. If this pathway dominates the excited-state dynamics, the low quantum yield is likely caused by rapid recombination of the TPPFe(II)/TPPFe(IV)=O subunits ("reclamping") before substrate binding. However, the OTA has also been interpreted as supporting a competing pathway, in which the LMCT state predominately disproportionates into a ligand-centred charge separated state composed of catalytically inactive TPPFe(III)$^+$ and TPPFe(III)-O$^-$ subunits (Figure 1B, Pathway B), with only a small population of active Fe(IV)-oxo species below the detection threshold of transient absorption measurements.[7]

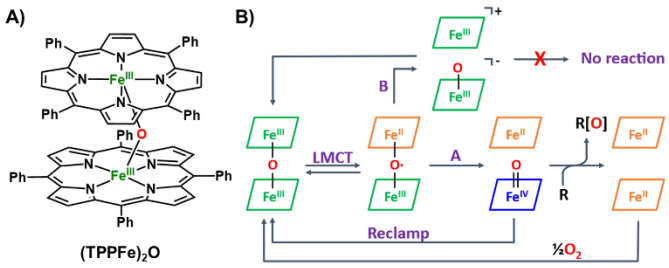

Figure 1 - (A) Structure of $(TPPFe)_2O$ (B) Proposed photocatalytic pathways in μ-oxo iron bisporphyrins.

[a] *Department of Chemistry, University of Illinois at Urbana-Champaign, 600 S. Mathews Ave., Urbana, Illinois 61801, USA..*

† *Authors contributed equally to this work.* Electronic Supplementary Information (ESI) available: for methods, sample preparation, additional experimental details and data. See DOI: 10.1039/x0xx00000x

Synthetic efforts in improving these quantum yields and efficiencies of these μ-oxo porphyrins have generally focused on increasing the lifetime and reactivity of the active transient iron(IV)-oxo intermediate, assuming that Pathway A dominates and that reclamping is the main source of low efficiency. These have included the development of "Pacman" porphyrins, which constrain the cleft conformation for favourable substrate coordination,[8–10] and introduction of electron-withdrawing groups[2] or corrole-based systems[11] to increase the oxidizing power of the iron centre. While these systems have shown improvements in overall reactivity, their quantum yields remain low ($<10^{-2}$). The OTA spectra of the Pacman porphyrins are similar to those of the unlinked μ-oxo iron porphyrins, and were interpreted as evidence for the iron(II)/iron(IV)-oxo state. However, assigning these transitions can be difficult, as the iron(II), iron(III), and iron(IV) porphyrin complexes share similar UV-Vis absorption features.[7] Although resonance Raman[12] and catalytic studies supported the formation of an iron(IV)-oxo species, they did not resolve whether the re-clamping of the iron(II)/iron(IV) state or the competing formation of inactive iron(III) ion pair state is the source of the low quantum yield.

In this work, we use femtosecond transient $M_{2,3}$-edge XANES spectroscopy and optical transient absorption to distinguish between the two proposed pathways in a simple μ-oxo bisporphyrin, $(TPPFe)_2O$, to identify the cause of its low quantum yield. $(TPPFe)_2O$ contains antiferromagnetically coupled high-spin Fe(III) porphyrins with a μ-oxo bridge between the iron centres, separated by a distance of about 5.2 Å.[13,14] Infrared, magnetic, and X-ray crystallographic studies[13] have shown that the iron centres in the stacked porphyrin have a structure akin to the high-spin iron in the monoporphyrin Fe(III)TPPCl. $(TPPFe)_2O$ has also been found to function as a photocatalyst for oxidation of triphenylphosphine[15] and cyclic alkenes[5] upon photoexcitation between 325 and 400 nm.[4,6,7,16] This molecule demonstrates similar pico- and nano-second dynamics as the more complex Pacman & Hangman porphyrins, so this simpler system serves as an excellent standard for the photodynamics of the u-oxo iron bisporphyrin systems.

We used femtosecond OTA spectroscopy to gain insight into the early dynamics after excitation of $(TPPFe)_2O$, supplementing prior later picosecond OTA studies and providing identification of the initial excited states. We then used transient $M_{2,3}$-edge XANES spectroscopy to probe the iron centres directly during their excited state dynamics. M-edge XANES measures the 3p-to-3d transition of first-row metals, and it provides comparable element, oxidation state, and ligand field specificity to L- and K-edge XANES.[17] This technique has been used to resolve the photophysics of several 3d metal systems,[18–20] including FeTPPCl. By interrogating the iron centre directly, we can identify its oxidation and spin-state directly during its photodynamics, and combined with femtosecond OTA spectroscopy, we can gain insight into the overall dominant photopathways after excitation. This will assist in determining the primary off-cycle pathway and informing potential alternate catalyst designs for increasing the quantum efficiency of these μ-oxo bimetallic systems for atom-efficient oxidation photocatalysis.

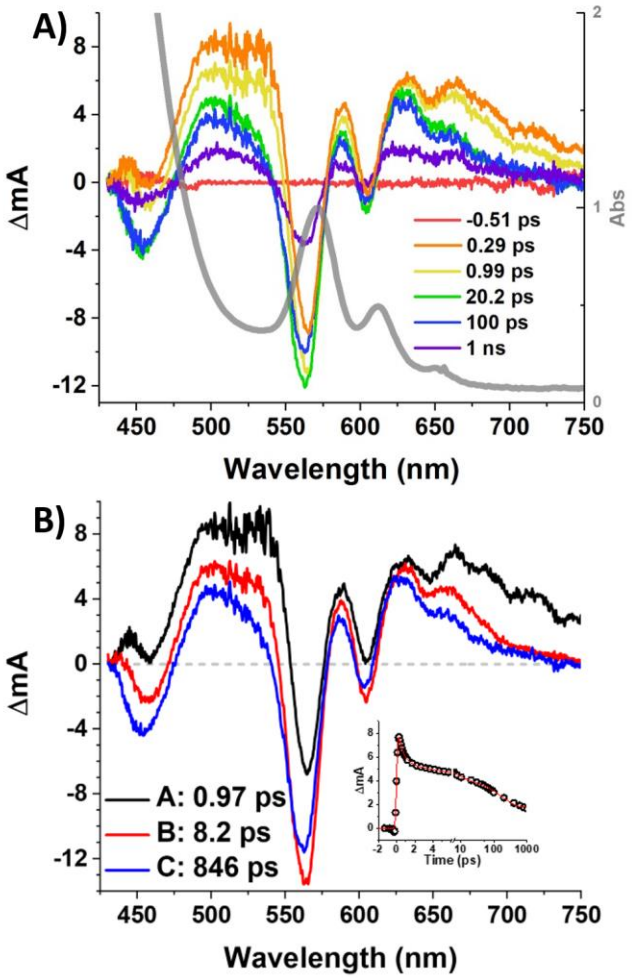

Figure 2 – (A) Optical transient absorption spectra of $(TPPFe)_2O$ (benzene) at select timepoints; grey trace is the static UV-Vis absorbance in benzene. (B) Component species associated difference spectra from global fit. Inset: Kinetic slice at 515 nm.

Results and Discussion

Optical transient absorption To examine the early photodynamics of $(TPPFe)_2O$ and complement prior picosecond studies, femtosecond optical transient absorption (OTA) spectroscopy was performed on a degassed benzene solution of the stacked porphyrin at 400 nm (see SI for experimental details). The ground state UV/Visible spectrum is shown in Figure 2A, along with transient spectra at selected delay times. Several key features are apparent in the transient spectra: positive absorption features from 620-750 nm, 575-600 nm, and 460-525 nm, and bleach features from 600-620 nm, 525-575 nm, and 460-440 nm. The strong bleach feature at 560 nm and weaker bleach feature at 605 nm correspond to Q-band bleaches when compared to the static UV-Vis (Figure 2A). The positive features centred at 515 nm and between 620 nm and 750 nm represent the formation of an excited state with new absorption features at these wavelengths. The bleach at 450 nm begins to appear after 1 ps and reaches its maximum intensity by ~20 ps. The delayed formation of this bleach suggests an

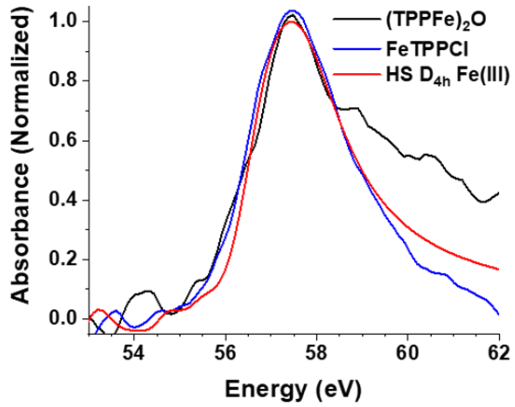

Figure 3 - Static $M_{2,3}$-edge spectra of $(TPPFe)_2O$, FeTPPCl, and ligand field multiplet simulation of a high-spin D_{4h} iron(III) centre.

initial excited state species that absorbs in this region and counteracts the ground state bleach. Additionally, between 100 fs and 2 ps, the positive feature from 650 nm to 750 nm decays significantly and the 560 nm Q-band bleach feature increases intensity. Over the next 10-20 ps, absorption feature near 620 nm sharpens and the other features become slightly more negative. This spectrum then decays slowly over the next nanosecond, with significant intensity remaining at the end of the experimental 1 ns time window. These long-lived features match well with prior OTA studies of $(TPPFe)_2O$. [7,4]

A global analysis of the transient spectra was performed using the program Glotaran.[21] A three-state A→B→C sequential model convolved with a Gaussian instrument response function (IRF) of 129 fs was required to model the excited state spectra. The species associated difference spectra (SADS) of each component are shown in Figure 2B, with an inset showing a kinetic slice of the data and the fit at 515 nm. Exponential lifetimes of 0.97 ± 0.02 ps, 8.2 ± 0.3 ps, and 846 ± 8 ps for states A, B, and C, respectively, were extracted from the fit. The final lifetime is only approximate given the 1 ns time window of the experiment. As shown in the S.I. (Figures S2- S9, Tables S1-S5), these dynamics do not change significantly upon excitation at 350 or 325 nm, or in other solvents, suggesting that the excited states evolution is relatively insensitive to the experimental conditions.

Based on our prior work with FeTPPCl,[20] we assign State A (not observed in earlier picosecond studies due their limited time resolution) as the LMCT excited state. The spectra of States B and C are similar to each other, but are markedly different from State A, featuring a bleach at 450 nm and lacking the broad absorption from 650-750 nm. We therefore assign B and C as vibrationally hot and cold versions of the same electronic state. This state was previously assigned as either the ion pair[7] or the Fe(II)/Fe(IV)-oxo state,[4,15,22] a disagreement which we will resolve with transient XANES below.

Iron $M_{2,3}$-edge XANES To identify the short-lived electronic states of the iron centres, we performed ultrafast transient Fe $M_{2,3}$-edge X-ray absorption near-edge spectroscopy (XANES). $M_{2,3}$-edge XANES measures the 3p-to-3d transition of first-row metals, and it provides comparable element, oxidation state, and ligand field specificity to L- and K-edge XANES.[17] This technique has been used to resolve the photophysics of several

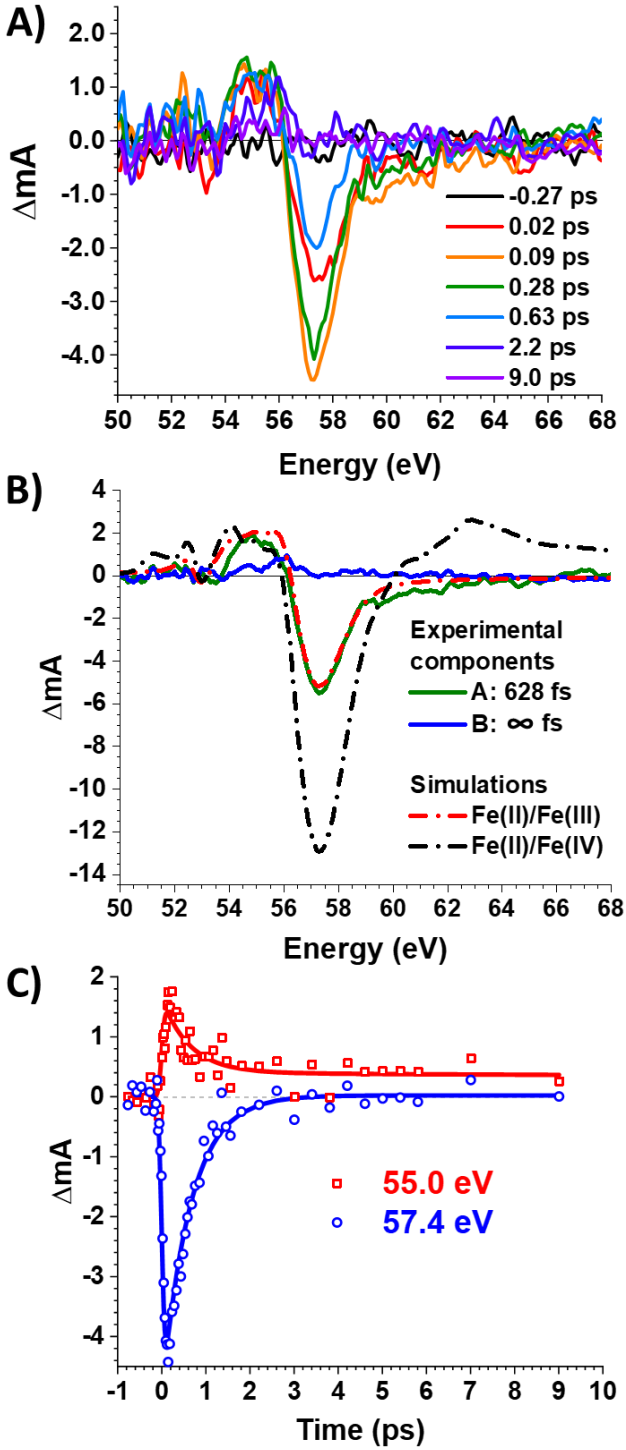

Figure 4 - Transient $M_{2,3}$-edge XANES of $(TPPFe)_2O$ with 400 nm excitation: (A) Spectral slices at select time points. (B) Comparison of spectral components (SADS) with simulated Fe(II)/Fe(IV) and Fe(II)/Fe(III) spectra given an 8% excitation fraction. (c) Kinetic traces at the 55.0 eV absorption and 57.4 eV bleach, with global fit traces.

3d metal systems,[18–20] including FeTPPCl. The broadband XUV probe was generated using high-harmonic generation (HHG) employing a tabletop instrument described previously.[17] For compatibility with the ultrahigh vacuum of the XUV spectrometer, the bisporphyrin was embedded in polystyrene film as a proxy for benzene solution.[23] As shown Figure S9 in the S.I., the kinetics measured by OTA are nearly identical between solution and film.

Figure 3 shows the ground-state iron $M_{2,3}$-edge XANES spectrum of $(TPPFe)_2O$, along with ligand field multiplet simulation of high-spin Fe(III) centre (additional simulations of Fe(II) and Fe(IV) in Figure S12). The ground-state spectrum of FeTPPCl is also shown as a reference molecule, and its spectrum is an excellent match for that of the bisporphyrin with a main peak at 57.4 eV and small pre-peaks between 54 and 56 eV. This similarity, as well as the good match of both Fe(III) complexes to the simulated Fe(III) spectrum, supports the assignment of each porphyrin centre as high-spin Fe(III).

As is common for XANES spectra, reduction of the metal centre causes a redshift in the overall spectrum due to increased screening that raises the energy of the 3p core level, and conversely oxidation of the metal centre causes a blueshift. The multiple peaks within a single spectrum are caused by coupling between the 3d electrons and the 3p core-hole, as is discussed in more detail in the Supporting Information. From this figure, we can predict that formation of that photoreduction of the ground-state Fe(III) centre to a Fe(II) centre will cause a net redshift in the XANES spectrum, while formation of a Fe(IV) centre will cause a net blueshift.

Transient $M_{2,3}$-edge XANES was performed after 400 nm excitation, with an excitation fraction of 8% per iron centre as estimated from the pump fluence of 1.6 mJ/cm^2 and molar absorptivity of ~100,000 M^{-1}cm^{-1} of the stacked porphyrin (i.e. two iron porphyrin centres). Figure 4A contains the spectral slices (pump-on minus pump-off) from -0.27 ps (before time zero) to 9.0 ps. Time zero is independently measured by performing transient absorption of α-Fe_2O_3. Upon excitation, a bleach feature centred at 57.4 eV appears along with a positive feature centred at 55.0 eV. By 2 ps, these features decay to a weak positive signal at 56.0 eV. A global fit to an A→B model (with B having an infinite lifetime on the 10 ps time window of this experiment) highlights these spectral components, as shown in Figure 4B. Kinetic traces at 55.0 and 57.4 eV are shown in Figure 4C. Component A rises with an instrument response function (IRF) of 146 ± 5 fs FWHM and decays with an exponential time constant of 638 ± 14 fs. This IRF is slightly longer than the 90 fs response measured using α-Fe_2O_3. Such a delayed rise was also observed in FeTPPCl and is caused by partial π-π^* character in the initial excited state, which relaxes in tens of fs to a fully LMCT state. The 638 fs decay of XUV state A is a reasonably good match to the 1 ps decay of OTA state A.

In order to assign the transient XANES spectrum, ligand field multiplet simulations[17,24,25] were performed for the potential Fe(II)/Fe(III) [LMCT] and Fe(II)/Fe(IV)-oxo states. Note that in the TPPFe(III)$^+$/TPPFe(III)-O$^-$ [ion pair] state, the irons' electronic structure has not changed significantly from the ground state, so only a weak transient signal is expected in the metal-specific XANES probe. These simulations are shown in Figure 4B and are scaled to the 8% excitation fraction. The LMCT state is predicted to have a ground state bleach at 57.4 eV caused by loss of Fe(III), and excited state absorptions at 53 and 55 eV caused by the formation of Fe(II). This simulation is a nearly quantitative match to the experimental spectrum of component A, both in magnitude and shape. The Fe(II)/Fe(IV)-oxo state is calculated to have a ground-state bleach at 57.4 eV about twice as large as that of the LMCT state because two Fe(III) signals are lost. The Fe(II) ion leads to positive absorption features at 53 and 55 eV, and the Fe(IV) causes a broad positive feature at 63 eV. The latter peak are not observed in the experimental spectrum, indicating that no Fe(IV) is formed with the signal-to-noise of the experiment. This weak positive signal in the long-lived state is consistent with ligand-centred excitation (either electronic or vibrational) that minimally perturbs the metal's d-orbital manifold.[20]

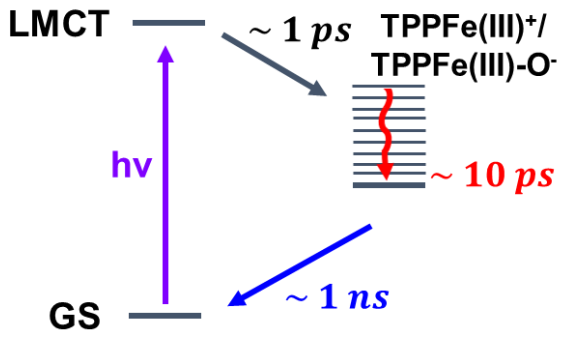

Figure 5 - Proposed dominant photodynamics for $(TPPFe)_2O$

Discussion By combining the OTA and XTA results, a consistent picture emerges of the dominant bisporphyrin excited state dynamics, which is summarized in Figure 5. Photoexcitation of the mixed π-π^*/LMCT band at 400 nm is followed by rapid relaxation into the Fe(II)/Fe(III) LMCT state (as shown by the delayed rise of the Fe(II) signal in XTA). This state decays to the TPPFe(III)$^+$/TPPFe(III)-O$^-$ ion pair in ~1 ps, as shown by the loss of the Fe(II) signal in XTA and the change in shape of the OTA spectrum. After vibrational cooling, the ion pair state lasts for approximately a nanosecond before recombining to the $(TPPFe)_2O$ ground state.

By using time-resolved M-edge XANES to probe the iron photocatalyst directly with complementary OTA studies, the photodynamics of these bisporphyrins can be elucidated and applied towards understanding the catalytic mechanism. Crucially, the use of M-edge XANES to track the transient change in oxidation states at the iron centres allowed for clear identification of the main photo-generated intermediate. Overall, our experimental picture shows that upon photoexcitation, the stacked porphyrin predominantly follows Pathway B in Figure 1A, formation of the ion pair state, and not Pathway A, where the TPPFe(II)/TPPFe(IV)=O state is formed but reclamps. While the activity of μ-oxo iron bisporphyrins suggests that the active Fe(IV)-oxo state is formed in at least small amounts,[4,12] the relative population compared to the ion pair state is low enough that it does not appear by the current experimental conditions. The disfavouring of the Fe(IV)-oxo state for the inactive iron(III) ion pair state explains the low quantum yield of product formation. Furthermore, it explains why past efforts to improve the lifetime of the Fe(IV)-oxo have not improved the quantum yield above a few percent: the rare formation of that state imposes a low ceiling on the yield. Significant improvements in the quantum yield are more likely to be obtained by improving the branching ratio of forming the Fe(IV)-oxo over the Fe(III) ion pair state. Synthetic modifications that disfavour the formation of the ion pair state could include

installing electron donating groups to favour stabilization of the Fe(IV)-oxo or desymmetrizing one of the porphyrins to favour the TPPFe(II)/TPPFe(IV)=O state. By destabilizing the ligand-centred ion pair, this may shift the excited-state branching toward the catalytically active Fe(IV) state and improve the overall quantum yield of these photocatalysts, making them more viable for sustainable photooxidation. Minor changes in the transient state lifetimes based on solvent polarity (SI Table S2-4) provides evidence that changing the local environment about the iron centres could influence the photodynamics of the bisporphyrin system, supporting the viability of ligand substitution as a method for changing the branching ratio. Integration of non-heme iron centres could also assist in favouring the Fe(II)/Fe(IV)-oxo state over the inactive Fe(III) ion pair state. Karlin and coworkers showed one of the first examples of a non-heme/heme μ-oxo bridged complex that could perform photooxidation, though the quantum yields were comparable to the fully heme-based systems.[11] A recent report[26] demonstrated a fully non-heme μ-oxo system for photoactivated methanol oxidation with improved quantum yields, with DFT indicating preferred formation of an active iron(IV)-oxo centre over iron(III) centres.

Conclusions

Bridged u-oxo iron bisporphyrins show potential for sustainable oxidation of substrates using simply light and O_2 without an external reductant. We investigated the photodynamics of a simple u-oxo system, $(TPPFe)_2O$, using transient optical and iron M-edge XANES spectroscopy, identifying the predominant formation of a ligand-centred iron(III) ion pair state as the likely source of the low quantum yields in these systems, instead of rapid reclamping of the iron(II)/iron(IV) state. This work highlights the utility of transient core-level spectroscopy in probing reaction mechanisms and identifying new avenues for catalyst design.

Conflicts of interest

There are no conflicts to declare.

Acknowledgements

This material is based upon work supported by the U.S. Department of Energy, Office of Science, Office of Basic Energy Sciences under Award Number DE-SC0018904. This material is based upon work supported by the National Science Foundation Graduate Research Fellowship under Grant No. DGE-1746047. K. Sye thanks the Springborn Fellowship. The transient XUV instrument was built with partial funding from the Air Force Office of Scientific Research under AFOSR Awards No. FA9550-14-1-0314 and FA9550-18-1-0293. We thank Alison R. Fout for insightful discussion and Yusef Shari'ati for global fitting help.

Notes and references

1 A. Maldotti, R. Amadelli, C. Bartocci, V. Carassiti, E. Polo and G. Varani, *Coord. Chem. Rev.*, 1993, **125**, 143–154.

2 J. Rosenthal, T. D. Luckett, J. M. Hodgkiss and D. G. Nocera, *J. Am. Chem. Soc.*, 2006, **128**, 6546–6547.

3 J. Rosenthal, B. J. Pistorio, L. C. Leng and D. G. Nocera, *J. Org. Chem.*, 2005, **70**, 1885–1888.

4 M. W. Peterson, D. S. Rivers and R. M. Richman, *J. Am. Chem. Soc.*, 1985, **107**, 2907–2915.

5 L. Weber, G. Haufe, D. Rehorek and H. Hennig, *J. Chem. Soc. Chem. Commun.*, 1991, 502–503.

6 M. W. Peterson and R. M. Richman, *Inorg. Chem.*, 1985, **24**, 722–725.

7 C. R. Guest, K. D. Straub, J. A. Hutchinson and P. M. Rentzepis, *J. Am. Chem. Soc.*, 1988, **110**, 5276–5280.

8 Y. Deng, C. J. Chang and D. G. Nocera, *J. Am. Chem. Soc.*, 2000, **122**, 410–411.

9 C. J. Chang, Y. Deng, A. F. Heyduk, C. K. Chang and D. G. Nocera, *Inorg. Chem.*, 2000, **39**, 959–966.

10 B. J. Pistorio, C. J. Chang and D. G. Nocera, *J. Am. Chem. Soc.*, 2002, **124**, 7884–7885.

11 I. M. Wasser, H. C. Fry, P. G. Hoertz, G. J. Meyer and K. D. Karlin, *Inorg. Chem.*, 2004, **43**, 8272–8281.

12 P. K. Shantha and A. L. Verma, *Inorg. Chem.*, 1996, **35**, 2723–2725.

13 A. B. Hoffman, D. M. Collins, V. W. Day, E. B. Fleischer, T. S. Snvastava and J. L. Hoard, *J. Am. Chem. Soc.*, 1972, **94**, 3620–3626.

14 E. B. Fleischer and T. S. Srivastava, *J. Am. Chem. Soc.*, 1969, **91**, 2403–2405.

15 R. M. Richman and M. W. Peterson, *J. Am. Chem. Soc.*, 1982, **104**, 5795–5796.

16 K. S. Suslick, J. F. Bautista and R. A. Watson, *J. Am. Chem. Soc.*, 1991, **113**, 6111–6114.

17 K. Zhang, M. F. Lin, E. S. Ryland, M. A. Verkamp, K. Benke, F. M. F. De Groot, G. S. Girolami and J. Vura-Weis, *J. Phys. Chem. Lett.*, 2016, **7**, 3383–3387.

18 K. Zhang, R. Ash, G. S. Girolami and J. Vura-Weis, *J. Am. Chem. Soc.*, 2019, **141**, 17180–17188.

19 S. Londo, S. Biswas, J. Husek, I. V. Pinchuk, M. J. Newburger, A. Boyadzhiev, A. H. Trout, D. W. McComb, R. Kawakami and L. R. Baker, *J. Phys. Chem. C*, 2020, **124**, 11368–11375.

20 E. S. Ryland, M.-F. Lin, M. A. Verkamp, K. Zhang, K. Benke, M. Carlson and J. Vura-Weis, *J. Am. Chem. Soc.*, 2018, **140**, 4691–4696.

21 J. J. Snellenburg, S. Laptenok, R. Seger, K. M. Mullen and I. H. M. van Stokkum, *J. Stat. Softw.*, 2012, **49**, 1–22.

22 J. M. Hodgkiss, C. J. Chang, B. J. Pistorio and D. G. Nocera, *Inorg. Chem.*, 2003, **42**, 8270–8277.

23 Y. Shari'ati and J. Vura-Weis, *J. Synchrotron Radiat.*, 2021, **28**, 1850–1857.

24 K. Zhang, G. S. Girolami and J. Vura-Weis, *J. Synchrotron Radiat.*, 2018, **25**, 1600–1608.

25 E. Stavitski and F. M. F. de Groot, *Micron*, 2010, **41**, 687–694.

26 J. Chen, S. Stepanovic, A. Draksharapu, M. Gruden and W. R. Browne, *Angew. Chemie Int. Ed.*, 2018, **57**, 3207–3211.